

Continuum Singularities of a Mean Field Theory of Collisions

B.G. Giraud

giraud@spht.saclay.cea.fr, Service de Physique Théorique, DSM, CE Saclay, F-91191 Gif/Yvette, France

and

A. Weiguny

weiguny@uni-muenster.de, Institut für Theoretische Physik, Universität Münster, D-48149 Münster, Germany

(November 20, 2018)

Consider a complex energy z for a N -particle Hamiltonian H and let χ be any wave packet accounting for any channel flux. The time independent mean field (TIMF) approximation of the inhomogeneous, linear equation $(z - H)|\Psi\rangle = |\chi\rangle$ consists in replacing Ψ by a product or Slater determinant ϕ of single particle states φ_i . This results, under the Schwinger variational principle, into self consistent TIMF equations $(\eta_i - h_i)|\varphi_i\rangle = |\chi_i\rangle$ in single particle space. The method is a generalization of the Hartree-Fock (HF) replacement of the N -body homogeneous linear equation $(E - H)|\Psi\rangle = 0$ by single particle HF diagonalizations $(e_i - h_i)|\varphi_i\rangle = 0$. We show how, despite strong nonlinearities in this mean field method, threshold singularities of the *inhomogeneous* TIMF equations are linked to solutions of the *homogeneous* HF equations.

I. INTRODUCTION

After the success of the mean field approach for bound state systems in various fields of physics, it was only natural to try the mean field concept for scattering states as well. The original attempt [1] was the time-dependent Hartree-Fock (TDHF) method where one solves the single-particle equations of motion as *initial* value problem in time. From the resulting solutions at various impact parameters one may then calculate the classical cross section. With no specification of the final state, the method is restricted to inclusive reactions. A serious, conceptual problem arises from spurious cross channel correlations [2,3]: when projecting the TDHF Slater determinant for large times on an orthogonal set of channel wave functions, the expansion coefficients and the respective S-matrix vary in time ad infinitum. To overcome the shortcomings of TDHF, the time-dependent mean field (TDMF) approach [2,3,4] expands the density in two sets of (bi-orthogonal) single-particle wave functions and solves the equations of motion as *boundary* value problem in time, fixing initial and final densities. It has been proven that for TDMF an S-matrix can be defined which becomes asymptotically constant [2]. The problem with TDMF lies in combining self-consistency with given boundary conditions in time [3,5]. No practicable algorithm for this highly “non-local” problem exists upto date for use in actual numerical calculations. A third approach is the time-independent mean field (TIMF) method [6], based on a Schwinger-type variational principle [7] for matrix elements of the resolvent or T-operator between given initial and final states. The method uses two sets of variational single-particle functions, analogous to TDMF, and leads to inhomogeneous equations of Hartree-Fock type which can be solved iteratively for given total energy of the system. TIMF is free of the conceptual and practical problems of TDHF and TDMF, resp., and has been tested successfully on a number of simple systems. It can be extended to incorporate particle-hole correlations, as has also been done for TDHF, within a generalized random-phase-approximation [8]. The present paper goes beyond the above problems [9] by studying the continuum singularities of this TIMF approach for collisions.

Consider a finite number N of particles. Factorized wave packets (shifted Gaussians in momentum representation for example) make an overcomplete basis in their Hilbert space of wavefunctions. Hence the calculation of a retarded Green’s function amplitude $\mathcal{D} \equiv \langle \chi | (z - H)^{-1} | \chi \rangle$, where *i*) χ is a product, $|\chi\rangle = \prod_{i=1}^N |\chi_i\rangle$, and *ii*) each single particle wave function χ_i is real rather than complex, makes a fully generic problem. Such factorization simplifications are not physically restrictive and help in the analysis of a mean field theory of collisions, the subject of this paper.

For the sake of simplicity, we deal yet with spinless, distinct particles only and short range interactions v_{ij} for the Hamiltonian $H = \sum_{i=1}^N p_i^2 / (2m_i) + \sum_{i>j=1}^N v_{ij}$. The case of identical particles can be treated later and, in the following, any reference to a Hartree method may be understood as a reference to a Hartree-Fock (HF) method if necessary. Again for simplicity, we consider the calculation of diagonal collision amplitudes only, $\langle \vec{k} | V (E^+ - H)^{-1} V | \vec{k} \rangle$, Born term subtracted. Generalizations to distinct prior and post interactions, V, V' , are kept for future work. The state $|\vec{k}\rangle$ is taken as a plane wave of relative motion in any two cluster channel ground state and the product $|\chi\rangle \equiv V |\vec{k}\rangle$ is

a square integrable state in the N -particle space. Finally z is any complex number $E + i\Gamma$, and the usual limit E^+ at the end of any calculation reads $\Gamma \rightarrow +0$.

It is trivial to use the Schwinger variational principle [7] and show that \mathcal{D} is the stationary value of the functional

$$\mathcal{F} \equiv \frac{\langle \Psi' | \chi \rangle \langle \chi | \Psi \rangle}{\langle \Psi' | (z - H) | \Psi \rangle}, \quad (1)$$

under variations of Ψ, Ψ' . The corresponding Euler-Lagrange equations read, with retarded boundary conditions and arbitrary norms and phases of Ψ and Ψ' ,

$$(z - H)|\Psi\rangle = |\chi\rangle, \quad \langle \Psi' | (z - H) = \langle \chi|. \quad (2)$$

The variational equations which occur in the time independent mean field (TIMF) [6] theory of collisions read,

$$(\eta_i - h_i)|\varphi_i\rangle = |\chi_i\rangle, \quad \langle \varphi'_i | (\eta_i - h_i) = \langle \chi_i|, \quad i = 1, \dots, N. \quad (3)$$

They are obtained from Eq. (1) when χ , and the approximation ϕ , resp. ϕ' , chosen for Ψ , resp. Ψ' , are products of single particle orbitals, $\chi_i, \varphi_i, \varphi'_i$, respectively. Such TIMF equations are very simple [6]. Except for a single particle density operator ρ defined non diagonally as $\rho(\vec{r}', \vec{r}) = \sum_i \varphi_i(\vec{r}') \varphi_i^*(\vec{r})$, they are just Hartree(-Fock) equations completed by a right hand side, representing the image of the channel in single particle space. In the following, \mathcal{F} is restricted to such factorized source functions χ and trial functions ϕ, ϕ' and will be labeled F . A saddle value under such a restriction of ϕ, ϕ' is not necessarily unique any more. It will be denoted by D instead of \mathcal{D} and may request an additional, identifying label. Now our claim is: *bound and unbound solutions of the usual Hartree(-Fock) equations,*

$$(e_i - h_i)|\varphi_i\rangle = 0, \quad (4)$$

induce singularities of the one-body variational conditions, Eqs. (3).

This reminds, naturally, of the strict connection between the singularities of the linear, inhomogeneous problem $(z - H)|\Psi\rangle = |\chi\rangle$ in the N -body space and the solutions of the linear, homogeneous Schrödinger equation $(E - H)|\Psi\rangle = 0$ in the same space. Because of the nonlinear nature of Eqs. (3-4) in single particle space, our claim is not obvious, and will be qualified in this paper.

Actually, in a previous paper [10], the claim was already substantiated in part : those energies E_H , for which a bound Hartree(-Fock) solution ϕ_H is found, generate poles of the approximate amplitude D provided by saddle points of the restriction F . Furthermore $(z - E_H)D \rightarrow |\langle \chi | \phi_H \rangle|^2 / \langle \phi_H | \phi_H \rangle$ when $z \rightarrow E_H$. Despite the nonlinearity of the approximation, such a residue at such a pole is almost expected. The analogy with the poles of \mathcal{D} at exact eigenvalues for bound states is striking. We are now interested in a more difficult question, namely, is there a similar analogy at higher energies, when singularities of scattering and rearrangement collisions (thresholds, cuts) occur?

In Section II we briefly recall a very simple, soluble model [11], used earlier among several other models to validate D as an approximation of \mathcal{D} . The model is reintroduced for pedagogical reasons first, to illustrate a derivation of Eqs. (3). Then, and mainly, it is used to provide a complete investigation of singularities, for it boils down to manipulations of polynomials. In Section III we introduce an enriched model, exactly soluble too. Section IV contains a generalization and discussion of the results obtained in Sections II and III. Finally Section V contains our conclusion.

II. FIRST MODEL, BARE PROPAGATION, SYMMETRIC MEAN FIELD, TWO-BODY THRESHOLD

In this soluble model, there are only two one-dimensional particles with just their kinetic energies, and different masses $m_i = 1/(2a_i)$, hence $H = a_1 p_1^2 + a_2 p_2^2$. While the inversion of $z - H$ is numerically trivial and allows a good validation [11] of the TIMF approximation, the formal expression of $(z - H)^{-1}$ in terms of one-body propagators $(\eta_1 - a_1 p_1^2)^{-1}$ and $(\eta_2 - a_2 p_2^2)^{-1}$ is less trivial, as it demands a convolution. The TIMF method consists in replacing the convolution by just one product, namely

$$(z - a_1 p_1^2 - a_2 p_2^2)^{-1} |\chi_1 \chi_2\rangle \propto (\eta_1 - a_1 p_1^2)^{-1} |\chi_1\rangle (\eta_2 - a_2 p_2^2)^{-1} |\chi_2\rangle. \quad (5)$$

This comes from variations $\delta/\delta\varphi_i$ of the functional F . An additional simplification results from a further remark : in those representations where χ and H are real, one finds from Eqs. (2) that $|\Psi'\rangle = |\Psi^*\rangle$, hence the possibility of just one trial function Ψ if one uses a Euclidian ($| \rangle$) rather than a Hermitian ($\langle | \rangle$) metric,

$$\mathcal{F} \equiv \frac{(\Psi|\chi)(\chi|\Psi)}{(\Psi|(z-H)|\Psi)} = \frac{(\chi|\Psi)^2}{(\Psi|(z-H)|\Psi)}. \quad (6)$$

For the present two particle model, the factorization of χ into two single particle wave packets with real wave functions χ_1, χ_2 allows us to use the following form of F ,

$$F = \frac{(\chi_1\chi_2|\varphi_1\varphi_2)^2}{(\varphi_1\varphi_2|(z-a_1p_1^2-a_2p^2)|\varphi_1\varphi_2)} = \frac{(\chi_1|\varphi_1)^2(\chi_2|\varphi_2)^2}{z(\varphi_1|\varphi_1)(\varphi_2|\varphi_2) - (\varphi_1|a_1p_1^2|\varphi_1)(\varphi_2|\varphi_2) - (\varphi_1|\varphi_1)(\varphi_2|a_2p_2^2|\varphi_2)}. \quad (7)$$

We assume that χ_1, χ_2 are real in the momentum representation. The functional being insensitive to the norms and global phases of φ_1, φ_2 , elementary manipulations of $\delta F/\delta\varphi_i$ yield, in the same momentum representation,

$$\varphi_i(p) = \frac{\chi_i(p)}{\eta_i - a_i p^2}, \quad i = 1, 2, \quad (8)$$

with

$$\eta_i = z - \frac{\int dp \varphi_j^2(p) a_j p^2}{\int dp \varphi_j^2(p)} = z - \eta_j - \frac{\int dp \chi_j^2(p)(a_j p^2 - \eta_j)^{-1}}{\int dp \chi_j^2(p)(a_j p^2 - \eta_j)^{-2}}, \quad i = 1, 2, \quad \text{and} \quad j = 1, 2, \quad \text{and} \quad j \neq i. \quad (9)$$

It is convenient at this stage to define the integrals,

$$I_i = -(\chi_i|\varphi_i) = \int dp \frac{\chi_i^2(p)}{a_i p^2 - \eta_i}, \quad i = 1, 2, \quad (10)$$

and notice that Eqs. (9) then read,

$$I_j \frac{d\eta_j}{dI_j} = z - \sum_{i=1}^2 \eta_i, \quad j = 1, 2. \quad (11)$$

If furthermore one defines auxiliary variables ω_i by the conditions

$$\eta_i = a_i \omega_i^2, \quad \Im \omega_i > 0, \quad i = 1, 2, \quad (12)$$

then it is useful to define $J_j \equiv a_j I_j$. And Eqs. (11) become,

$$2 a_j \omega_j J_j \frac{d\omega_j}{dJ_j} = z - \sum_{i=1}^2 a_i \omega_i^2, \quad j = 1, 2, \quad (13)$$

where a contour in the upper half plane of the complex variable p defines the integrals,

$$J_j = \int dp \frac{\chi_j^2(p)}{p^2 - \omega_j^2}, \quad j = 1, 2. \quad (14)$$

The special cases $\Im \eta_j \rightarrow 0$ while $\Re \eta_j \geq 0$ define cuts in the complex η_j -plane. These correspond to $\Im \omega_j \rightarrow 0$ in the ω_j -plane.

When the two particles are identical, it may be interesting to symmetrize and antisymmetrize Eqs. (13) as,

$$\sum_{i=1}^2 a_i \omega_i J_i \frac{d\omega_i}{dJ_i} = z - \sum_{i=1}^2 a_i \omega_i^2, \quad (15)$$

and

$$a_1 \omega_1 J_1 \frac{d\omega_1}{dJ_1} - a_2 \omega_2 J_2 \frac{d\omega_2}{dJ_2} = 0, \quad (16)$$

and identify cases where the mean field might break their symmetry. But we shall keep the particles, and/or their channel wave packets, distinct for a while.

A soluble model, involving only the manipulation of polynomials, is obtained if one chooses the forms of the wave packets as follows,

$$\chi_j(p) = \left[\frac{\gamma_j}{\pi [(p - K_j)^2 + \gamma_j^2]} \right]^{1/2}, \quad j = 1, 2, \quad (17)$$

yielding the simple result,

$$J_j = \frac{i\gamma_j}{\omega_j[(\omega_j - K_j)^2 + \gamma_j^2]} + \frac{1}{(K_j + i\gamma_j)^2 - \omega_j^2} = \frac{-\omega_j - i\gamma_j}{\omega_j(\omega_j - K_j + i\gamma_j)(\omega_j + K_j + i\gamma_j)}. \quad (18)$$

Resulting polynomial equations turn out to have a lower degree if $K_j = 0$, for then J_j becomes $J_j = -1/[\omega_j(\omega_j + i\gamma_j)]$. As will be found in this and the next Sections, two kinds of singularities emerge, *i*) “physical” ones, which essentially depend on z and are not very sensitive to “technical” parameters K_j, a_j, γ_j , and *ii*) “technical” singularities, more sensitive to such parameters. The analytical continuation provided across η cuts [12] by this ω representation is clear.

Once Eqs. (13) have been solved, the saddle point values of the functional read, using Eqs. (7-11),

$$D = \frac{(a_1\omega_1^2 + a_2\omega_2^2 - z)J_1J_2}{a_1a_2}. \quad (19)$$

The search for singularities of D as a function of the physical energy z thus consists in eliminating ω_1, ω_2 between Eqs. (13) and Eq. (19). The former read, after elementary manipulations which take advantage of Eq. (18) when $K_1 = K_2 = 0$,

$$2a_1x^2y + a_1\gamma_2x^2 - a_2\gamma_2y^2 + 2yz + \gamma_2z = 0, \quad 2a_2y^2x + a_2\gamma_1y^2 - a_1\gamma_1x^2 + 2xz + \gamma_1z = 0, \quad (20)$$

where it was convenient to set $\omega_1 = ix$, $\Re x > 0$, and $\omega_2 = iy$, $\Re y > 0$. Equivalently, if we scale x and y into $x = \gamma_1x'$ and $y = \gamma_2y'$, respectively, the same equations read,

$$(A_1x'^2 + z)(1 + 2y') - A_2y'^2 = 0, \quad (A_2y'^2 + z)(1 + 2x') - A_1x'^2 = 0, \quad (21)$$

with $A_1 \equiv a_1\gamma_1^2$ and $A_2 \equiv a_2\gamma_2^2$. An elimination of y between Eqs. (20) gives,

$$2a_1^3\gamma_1x^7 - a_1^2(4z - a_1\gamma_1^2 + a_2\gamma_2^2)x^6 - a_1z(8z - a_1\gamma_1^2 + 4a_2\gamma_2^2)x^4 - 2a_1\gamma_1z(3z + a_2\gamma_2^2)x^3 - z^2(4z + a_1\gamma_1^2 + 4a_2\gamma_2^2)x^2 - 4z^2\gamma_1(z + a_2\gamma_2^2)x - \gamma_1^2z^2(z + a_2\gamma_2^2) = 0, \quad (22a)$$

$$y = -\frac{\gamma_2(a_1x^3 + 2xz + \gamma_1z)}{(2x + \gamma_1)(a_1x^2 + z)}. \quad (22b)$$

The multiplicity of solutions is thus 7, which raises a problem for the identification of a solution, if possible unique, which accounts for a physical approximation.

In turn, if one inserts Eq. (18) into Eq. (19), one obtains D as a rational function of ω_1, ω_2 , or x, y as well. Upon taking advantage of Eq. (22b), this rational fraction reduces into a rational fraction of x only, hence a polynomial relation between D and x , with degree 1 for D ,

$$a_1^2a_2\gamma_2^2x^3(\gamma_1 + x)^2(a_1x^3 + \gamma_1z + 2xz)D = 4a_1^3x^7(x + \gamma_1) + a_1^2(a_1\gamma_1^2 + a_2\gamma_2^2 + 12z)x^6 + 12a_1^2\gamma_1zx^5 + a_1z(3a_1\gamma_1^2 + 4a_2\gamma_2^2 + 12z)x^4 + 2a_1\gamma_1z(a_2\gamma_2^2 + 6z)x^3 + z^2(3a_1\gamma_1^2 + 4a_2\gamma_2^2 + 4z)x^2 + 4\gamma_1z^2(a_2\gamma_2^2 + z)x + \gamma_1^2z^2(a_2\gamma_2^2 + z). \quad (23)$$

The same result is obtained if one uses Eq. (7) instead of Eq. (19).

An elimination of x between Eq. (23) and Eq. (22a) finally gives a direct, polynomial condition relating D and z ,

$$\begin{aligned} & z_1^2z_2^2(z_1 + 1)(z_2 + 1)(z_1 + z_2 + 1)\bar{D}^7 - 4z_1z_2(z_1 + 1)(z_2 + 1)(z_1z_2 - 4z_1 - 4z_2 - 4)\bar{D}^6 - 4[3z_1^3z_2^2 + 3z_1^2z_2^3 + \\ & (20z_1^3z_2 + 58z_1^2z_2^2 + 20z_1z_2^3) + (16z_1^3 + 88z_1^2z_2 + 88z_1z_2^2 + 16z_2^3) + (32z_1^2 + 84z_1z_2 + 32z_2^2) + 16(z_1 + z_2)]\bar{D}^5 + \\ & 16[3z_1^2z_2^2 + 39(z_1^2z_2 + z_1z_2^2) + (32z_1^2 + 91z_1z_2 + 32z_2^2) + 48(z_1 + z_2) + 16]\bar{D}^4 + \\ & 16[3z_1^2z_2 + 3z_1z_2^2 - (8z_1^2 + 91z_1z_2 + 8z_2^2) - 88(z_1 + z_2) - 64]\bar{D}^3 + \\ & 192[-z_1z_2 + 4(z_1 + z_2) + 8]\bar{D}^2 - 64(z_1 + z_2 + 16)\bar{D} + 256 = 0, \end{aligned} \quad (24)$$

where $z_i = a_i\gamma_i^2/z$ and D is scaled as $D = \bar{D}/z$. The degree 7 for x in Eq. (22a) is correctly reflected here by the same degree for D (and \bar{D}). Conversely, given an amplitude D , the degree of the polynomial condition, Eq. (24),

with respect to z is 4. Hence there are 7 approximate amplitudes offered by TIMF for each energy, while the inverse problem, “given the TIMF amplitude, find the energy”, has 4 solutions.

This model, although soluble, thus creates a complicated Riemann surface. Criteria are necessary to select one physical sheet, or physical pieces of sheets. Obvious candidates are the conditions $\Re x \geq 0, \Re y \geq 0$ when Eqs. (20) are solved. Concerning Eq. (24), the very definition of \mathcal{D} demands that \mathcal{D} be real and negative if z is real and negative. When $z > 0$ with a slight and positive imaginary part, then $\Im \mathcal{D}$ must be negative. Those roots D which show the same properties should thus help the identification of suitable sheets.

The argument is made much simpler if the “technical” parameters $a_1\gamma_1^2$ and $a_2\gamma_2^2$ are taken equal to some common value θ . This amounts, in some sense, to consider identical particles, although a_1 may still differ from a_2 . Then Eq. (24) factorizes as

$$[4 - 4(\theta + z)D + \theta(\theta + z)D^2]^2 [16 + 8(3\theta - 4z)D + 4(3\theta^2 + 10\theta z + 4z^2)D^2 + \theta^2(2\theta + z)D^3] = 0. \quad (25)$$

If θ is used as a unit for z and similarly $1/\theta$ is used as a unit for D this reads as well,

$$[4 - 4(1 + z)D + (1 + z)D^2] = 0, \quad (26a)$$

$$[16 + 8(3 - 4z)D + 4(3 + 10z + 4z^2)D^2 + (2 + z)D^3] = 0. \quad (26b)$$

The presence of a squared polynomial as the first factor in Eq. (25) reflects a “symmetry breaking” by the mean field approximation. Indeed, when analyzing the corresponding solutions of Eqs. (20), one finds that each pair of roots $\{x, y\}$, with $x \neq y$, is accompanied by a pair $\{y, x\}$, generating the same value of D . Such a degeneracy thus makes, out of 4 of all the 7 solutions for $\{x, y\}$, two distinct values for D . All told, D then takes 5 distinct values. The remaining 3 solutions account for the degree 3 present in the second factor of Eq. (25). It is easy to verify that such 3 solutions are “symmetric”, namely $x = y$. Notice that the symmetry breaking generates a rational inverse function,

$$z_{bk} = \frac{(D_{bk} - 2)^2}{D_{bk}(4 - D_{bk})}, \quad (27)$$

while the symmetry conservation generates an equation of degree 2 for z . Since z_{bk} must be counted twice, one recovers the 4 solutions of the inverse problem.

It turns out that the “symmetry breaking” sector violates the double condition, $\Re x > 0, \Re y > 0$. Hence the properties of this sector are listed in an Appendix only. Turning now to the symmetric amplitude D_{sy} , the choice of a physical branch is reasonably easy, see Figs. 1-2. In Fig. 1, the lower half plane contains a loop acceptable as a physical candidate. We verified that $\Re x > 0$ for this loop. Despite a suitable $\Re x > 0$ if $z > 0$, the other branch in Fig. 1 is clearly not acceptable, for it contains values D_{sy} with positive imaginary parts. Nor can one accept the third branch, seen in Fig. 2, despite its correct sign for $\Im D_{sy}$. For it violates both the limit $\mathcal{D} \rightarrow 0$ when $|z| \rightarrow \infty$ and the obvious condition “ $\Re \mathcal{D} < 0$ if z is real and negative”. Furthermore $\Re x$ is found unsatisfactory for this third branch.

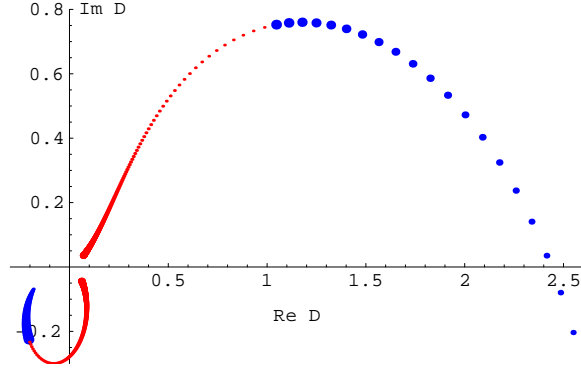


FIG. 1. Complex D -plane. Two trajectories of symmetry conserving amplitudes as functions of $\Re z$ when $\Im z = 1$. Growing blue dots: $\Re z$ grows from $-\infty$ to -0 . Growing red dots: $\Re z$ increases from $+0$. The third trajectory lies far in the lower half. Color is available online at www-spht.cea.fr/articles/t02/148/

Two values of z generate branching for D_{sy} . With a single root $D = -1/5$, reasonable, a double root $D = 16$, unphysical, occurs for $z = -27/16$, with expansion $D = 16 - 256/9 (z + 27/16) \pm 8192/243 [-(z + 27/16)^3]^{1/2}$. Hence a familiar square root cut can be used to disentangle the two corresponding sheets, both unphysical. The value $z = -27/16$ does not represent a natural threshold for the present model. More physical, obviously, is the triple root singularity, $D = -2$, which occurs at $z = 0$, the true threshold. It is illustrated by Fig. 3, where a tiny imaginary part $\Im z = .0001$ was added in order to separate branches. It will be noticed here that, although the physical branch gives real values of D_{sy} when $z < 0$ and complex values of the same when $z > 0$, there are always one real root and two complex conjugate roots on both sides in the vicinity of $z = 0$. This happens indeed because the corresponding discriminant, $\Delta_3 = 256z^2(27 + 16z)^3/(2 + z)^4$, actually changes sign, not for $z = 0$, but rather for $z = -27/16$. This helps to understand the nature of the unphysical singularity occurring at $z = -27/16$. It gives an early “warning” of the (cubic) physical threshold singularity, $z = 0$. An elementary, but slightly tedious calculation provides the expansions of the 3 branches in the vicinity of $z = 0$, namely $D = -2 - j 2^{2/3} 3 z^{1/3} + \mathcal{O}(z^{2/3})$, where j is either 1, or any one of its complex cubic roots $(-1 \pm i\sqrt{3})/2$.

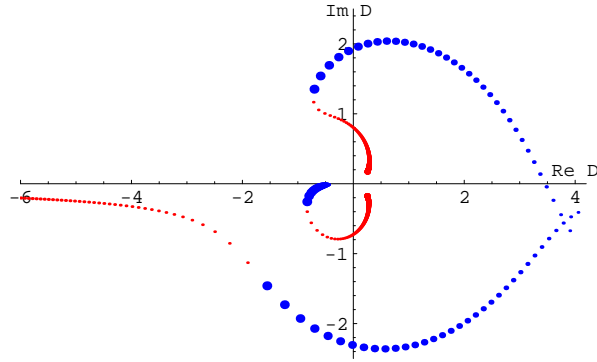


FIG. 2. Complex D -plane. All trajectories D_{sy} when $\Im z = .075$. Scales of trajectories made compatible by replacing radii from the origin by their square roots. Hence, for instance, announcing the double root $D = 16$ when $z = -27/16$, blue branches cross each other near $\sqrt{D} = 4$. Growing blue dots: $\Re z$ grows from $-\infty$ to -0 . Growing red dots: $\Re z$ increases from $+0$.

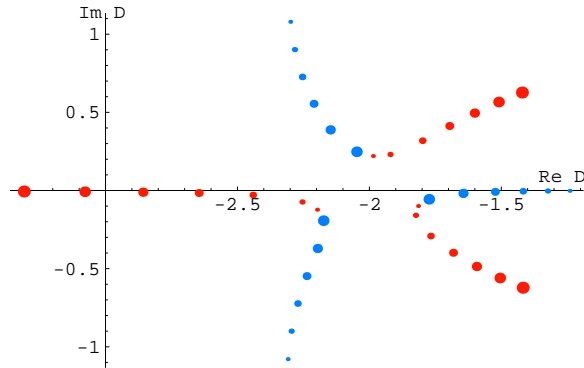


FIG. 3. Complex D -plane. Triple merging $D_{sy} \rightarrow -2$, with $\Im z = .0001$, $-.09 < \Re z < .09$. Lower right branch physical.

Consider Eqs. (21) and set $A_1 = A_2$ to factorize the resultant, Eq. (22a). Then scale x , y and z as proportional to γ_1 , γ_2 and A_1 , respectively. For the sake of simple numbers, this strictly amounts to set a common value $a_1 = a_2 = \gamma_1 = \gamma_2 = 1$, hence $A_1 = A_2 = 1$, for those reduced equations which govern the scaled variables and parameters. For the symmetry sector, $x = y$, both equations, Eqs. (20), then boil down to $2x^3 + 2xz + z = 0$. It is trivial to find that, at threshold $z \rightarrow 0$, all three roots have a leading term $x = (-z/2)^{1/3} + \mathcal{O}(z^{2/3})$, while, as already found, $D_{sy} = -2 + \mathcal{O}(z^{1/3})$. Obviously, below threshold, one must select the real root x , which gives a real amplitude. Conversely, above threshold, one must select that complex x which gives a retarded amplitude.

All told, for D_{sy} , cuts needed in the z -plane are a cut from 0 to $+\infty$ for the cubic branching and, for instance, a “technical” cut from $-\infty$ to $-27/16$ to create an additional seam between the second and the third sheets.

Now we consider additional cuts, namely those created by the condition $\Im\omega = 0$, or, identically, by the condition $\Re x = 0$. These occur because the solutions of realistic problems demand numerical, iterative calculations of η_i and φ_i before obtaining D . This means inversions of operators $(a_i\omega_i^2 - h_i)$ in sequences of successive approximations of ω 's (and self consistent h 's when potentials are involved). Obviously, every time $\Im\omega$ vanishes or becomes too small, numerical precautions are in order. Also, since the physical energy is on shell, $z = E + i0^+$, with a retardation boundary condition for many-body propagation, one would feel more comfortable with retardation also for the single particle energies $\eta \propto \omega^2$. Advanced η 's are not to be ruled out *a priori*, because it is well known that mean field approximations can be excellent while breaking many-body symmetries. But, clearly, branches of x 's which cross such cuts $\Re x = 0$ deserve some cautious scrutiny.

For the present case where $A_1 = A_2$ for “symmetric” bare propagations, and still with simple numbers $a_i = \gamma_i = 1$, our results are shown in Figs. 4-5. (For the academic, “symmetry breaking” case, see the Appendix with Figs. 13-14.) Fig. 4 is a contour plot of the product $\Re x_1 \Re x_2 \Re x_3$ of the real parts of the 3 roots as functions of z in the z -plane. Darker areas indicate an increasing positive product (two out of the three $\Re x$'s are < 0), while the lighter areas mean a more and more negative one (one negative $\Re x$ only). The product vanishes along the contour line separating the light grey area from the moderate grey one. It will be noticed that this line contains the point $z = 0$. Hence the cut relevant to D and that relevant to x 's both contain the two-body threshold. Notice, however, that, except at such a threshold, a real z induces complex η 's. Namely, propagation energy cuts *do not follow the real axis* in the z -plane.

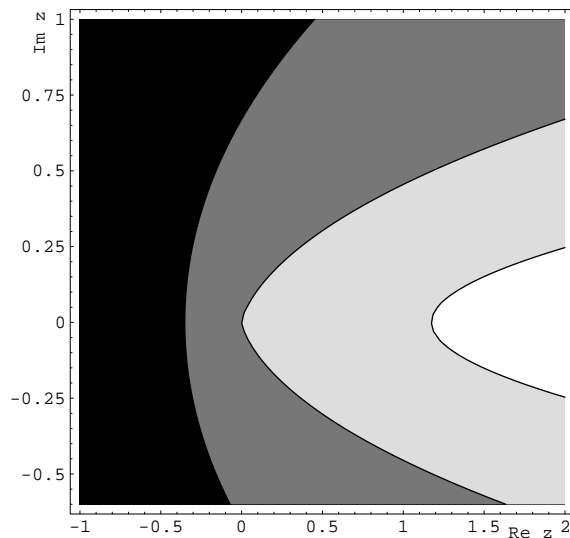


FIG. 4. Complex z -plane. Cut caused by the condition $\Re x = 0$ for symmetry conserving roots. The cut is the contour line separating the lighter grey area from the darker grey one.

The next Figure, Fig. 5, shows the trajectories of the roots when we freeze $\Re z = 0.1$, above threshold, and let $\Im z$ run from -1 to $+1$, hence allowing one $\Re x$, then a second one, to change their signs. The sizes of dots are coded as

follows: minimal for $\Im z = -1$, growing until $\Im z = 0$, minimal again for small positive values of $\Im z$, then growing again until $\Im z = 1$. The lower branch is the best candidate for physical roots, because it provides a growing retardation, $0 < \Im \eta \equiv \Im(-x^2)$, when $\Im z$ is positive and grows. As predicted from Fig. 4, there is an interval for $\Im z$ where 2 roots x have a positive $\Re x$.

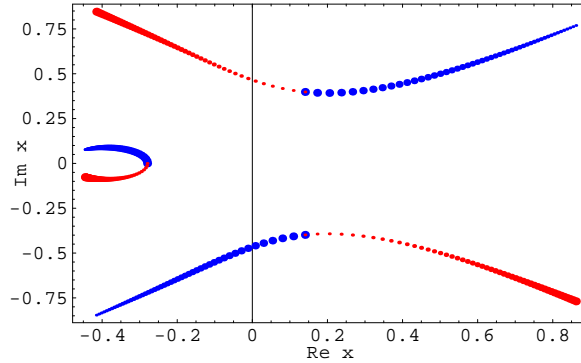


FIG. 5. Complex x -plane. Trajectories of the symmetry conserving x 's when $\Re z = 0.1$, while $\Im z$ crosses the cut shown by Fig. 4. Blue dots growing when $\Im z$ grows from -1 to 0 . Red dots growing when $\Im z$ grows from 0 to 1 .

To conclude this Section, the main result derived from this elementary model with bare propagation of two particles lies in the systematic, *physical*, two-body threshold found at $z = 0$ in the energy plane (z -plane) for all the mean field quantities, whether amplitudes D or propagation energies η . This threshold is, obviously, a common feature of both the exact problem and the corresponding Hartree problem. For amplitudes D , a cut in the z -plane extends from the threshold 0 to $+\infty$, as seen in both the “symmetric” and “breaking” submodels. For propagation energies η , the cut starts from $z = 0$, indeed, but deviates from the real semi-axis. For both D 's and η 's, the cost of the nonlinearity of the TIMF approach is reflected in additional, unphysical, “technical” singularities. But such unphysical singularities are not beyond interpretation either, as shown by the analytical properties listed in this Section. Incidentally, as discussed earlier [13], unphysical singularities may be washed out by a linear admixture of the various solutions of the nonlinear mean field problem. The next Sections will show even better how physical cuts remain a significant feature of the TIMF approximation.

III. SECOND SOLUBLE MODEL, ONE-BODY THRESHOLD

Here again we consider two one-dimensional particles, and particle 2 is still free with a pure kinetic energy $h_2 = a_2 p_2^2$ for its Hamiltonian. But now the complete Hamiltonian $H = h_1 + h_2$, while still separable, involves a bound state for particle 1, because we set $h_1 = a_1 p_1^2 - \lambda |\chi_1\rangle\langle\chi_1|$, with an attractive enough potential. For technical reasons which will soon become clear, the form $\lambda |\chi_1\rangle\langle\chi_1|$ of this potential makes use of the same wave packet χ_1 taken as a channel wave packet. The numerical inversion of $z - H$ is still easy and allows another good validation of the TIMF approximation. The formal expression of $(z - H)^{-1}$ in terms of one-body propagators $(\eta_1 - h_1)^{-1}$ and $(\eta_2 - h_2)^{-1}$ demands again a convolution and the TIMF method consists in replacing the convolution by a product,

$$(z - h_1 - h_2)^{-1} |\chi_1 \chi_2\rangle \propto (\eta_1 - h_1)^{-1} |\chi_1\rangle (\eta_2 - h_2)^{-1} |\chi_2\rangle. \quad (28)$$

This comes again from variations $\delta/\delta\varphi_i$ of the functional F . And a further remark can be repeated: in those representations where χ and H real, we obtain $|\Psi'\rangle = |\Psi^*\rangle$, see Eqs. (2). Hence the possibility of just one trial function ϕ under a Euclidian rather than a Hermitian metric, see Eq. (6). The factorization of χ into two real wave packets χ_1, χ_2 essentially retains Eq. (7), which actually becomes,

$$F = \frac{(\chi_1\chi_2|\varphi_1\varphi_2)^2}{(\varphi_1\varphi_2|(z-h_1-h_2)|\varphi_1\varphi_2)} = \frac{(\chi_1|\varphi_1)^2(\chi_2|\varphi_2)^2}{z(\varphi_1|\varphi_1)(\varphi_2|\varphi_2) - (\varphi_1|h_1|\varphi_1)(\varphi_2|\varphi_2) - (\varphi_1|\varphi_1)(\varphi_2|h_2|\varphi_2)}. \quad (29)$$

We use the same χ_1, χ_2 , real in the momentum representation. The functional being always insensitive to the norms and global phases of φ_1, φ_2 , the same manipulations of $\delta F/\delta\varphi_i$ yield, in the same momentum representation,

$$|\varphi_1\rangle = (\eta_1 - h_1)^{-1}|\chi_1\rangle, \quad (\eta_1 - a_1p_1^2)|\varphi_1\rangle = |\chi_1\rangle - \lambda|\chi_1\rangle(\chi_1|\varphi_1), \quad \varphi_1(p) = \frac{\chi_1(p)}{\eta_1 - a_1p^2} [1 - \lambda(\chi_1|\varphi_1)], \quad (30)$$

$$\varphi_2(p) = \frac{\chi_2(p)}{\eta_2 - a_2p^2}, \quad (31)$$

where it is better, temporarily at least, to retain the factor $\nu = [1 - \lambda(\chi_1|\varphi_1)]$ for φ_1 . The same quantity ν , as will be seen shortly, cannot be discarded from the self consistency conditions of the pair η_1, η_2 ,

$$\eta_1 = z - \frac{\int dp \varphi_2^2(p) a_2p^2}{\int dp \varphi_2^2(p)} = z - \eta_2 - \frac{\int dp \chi_2^2(p)(a_2p^2 - \eta_2)^{-1}}{\int dp \chi_2^2(p)(a_2p^2 - \eta_2)^{-2}}, \quad (32)$$

$$\eta_2 = z - \frac{(\varphi_1|h_1|\varphi_1)}{(\varphi_1|\varphi_1)} = z - \eta_1 - \frac{(\varphi_1|(h_1 - \eta_1)|\varphi_1)}{(\varphi_1|\varphi_1)} = z - \eta_1 - \frac{(\chi_1|(h_1 - \eta_1)^{-1}|\chi_1)}{(\chi_1|(h_1 - \eta_1)^{-2}|\chi_1)}. \quad (33)$$

Indeed, it is necessary to consider the matrix element,

$$\mathcal{I}_1 = (\chi_1|(h_1 - \eta_1)^{-1}|\chi_1), \quad (34)$$

and notice that Eqs. (32-33) become,

$$I_2 \frac{d\eta_2}{dI_2} = z - \eta_1 - \eta_2 = -\frac{(\chi_2|\varphi_2)}{(\varphi_2|\varphi_2)}, \quad \mathcal{I}_1 \frac{d\eta_1}{d\mathcal{I}_1} = z - \eta_1 - \eta_2 = -\frac{(\chi_1|\varphi_1)}{(\varphi_1|\varphi_1)}. \quad (35)$$

The integrals I_1, I_2 were already defined by Eq. (10). Returning to \mathcal{I}_1 , and to the factor ν which accounts for the separable potential present in h_1 , an elementary manipulation of Eq. (30) gives,

$$(\chi_1|\varphi_1) = -\mathcal{I}_1, \quad \mathcal{I}_1 = \frac{I_1}{1 - \lambda I_1}. \quad (36)$$

Again we define auxiliary variables ω_i by Eq. (12) and integrals $J_j \equiv a_j I_j$ by contours in the upper half plane of the complex variable p . Then Eqs. (35) become

$$2 a_2 \omega_2 J_2 \frac{d\omega_2}{dJ_2} = z - a_1 \omega_1^2 - a_2 \omega_2^2, \quad 2 a_1 \omega_1 \mathcal{I}_1 \frac{d\omega_1}{d\mathcal{I}_1} = z - a_1 \omega_1^2 - a_2 \omega_2^2. \quad (37)$$

It will be recalled here that a (unique) bound state occurs for h_1 for any positive value of λ , at an energy $\eta_0 < 0$, defined by the well known condition,

$$\frac{1}{\lambda} = \int dp \frac{\chi_1^2(p)}{a_1 p^2 - \eta_0} = \frac{J_1(\omega_0)}{a_1}, \quad \eta_0 = a_1 \omega_0^2, \quad \Re \omega_0 = 0, \quad \Im \omega_0 > 0. \quad (38)$$

Indeed, the right hand side is monotonically increasing when η_0 runs from $-\infty$ to 0 and the same r.h.s. diverges at $\eta_0 = 0$, see Eq. (18), because of our choice of a Lorentzian form for χ_1^2 . Accordingly, an explicit form of Eq. (38) is,

$$\lambda + a_1 \omega_0 (\omega_0 + i\gamma_1) = 0, \quad \Re \omega_0 = 0, \quad \Im \omega_0 > 0, \quad (39)$$

or, in terms of η_0 ,

$$(\eta_0 + \lambda)^2 + a_1 \gamma_1^2 \eta_0 = 0, \quad (40)$$

with obvious scaling properties. (Indeed, if the scale is set by λ for instance, it is convenient to define $A_1 = a_1\gamma_1^2$, and the relevant scales are, obviously, A_1/λ and η_0/λ .) Threshold singularities are expected for Eqs. (32-33) when z reaches the one-body threshold η_0 , besides the already found two-body threshold $z = 0$.

The saddle point value D deduced from Eq. (29) reads, upon taking advantage of Eqs. (30-37),

$$D = (a_1\omega_1^2 + a_2\omega_2^2 - z) \mathcal{I}_1 \mathcal{I}_2. \quad (41)$$

This formula, Eq. (41), is an obvious generalisation of Eq. (19). In the same way as we did in the previous Section, we shall again eliminate ω_1 and ω_2 , or rather the strictly equivalent variables $x = -i\omega_1$ and $y = -i\omega_2$, between Eqs. (37) and Eq. (41). It is then useful to define a parameter $A_2 = a_2\gamma_2^2$, quite similar to A_1 and it is also easy to predict that the solution $D(z)$ scales in terms of A_1/λ , A_2/λ , z/λ and λD . The Lorentzian choice for χ_1, χ_2 , induces the following forms for Eqs. (37), when we replace a_1, a_2 by $A_1/\gamma_1^2, A_2/\gamma_2^2$, respectively,

$$A_1\gamma_2^2x^2 + 2A_1\gamma_2x^2y - A_2\gamma_1^2y^2 + \gamma_1^2\gamma_2^2z + 2\gamma_1^2\gamma_2yz = 0, \quad (42a)$$

$$2\gamma_1\gamma_2^2\lambda x + A_2\gamma_1^2y^2 + 2A_2\gamma_1xy^2 - A_1\gamma_2^2x^2 + \gamma_1^2\gamma_2^2z + 2\gamma_1\gamma_2^2xz = 0, \quad (42b)$$

$$\frac{y}{\gamma_2} = - \frac{(\lambda\gamma_1^2 + A_1x^2)x + (\gamma_1 + 2x)\gamma_1^2z}{(\gamma_1 + 2x)(A_1x^2 + \gamma_1^2z)}. \quad (42c)$$

These scale obviously in terms of x/γ_1 and y/γ_2 . It is then convenient to set $\gamma_1 = \gamma_2 = 1$ in Eqs. (42).

Simultaneously, under the same replacement of a_1, a_2 by $A_1/\gamma_1^2, A_2/\gamma_2^2$, respectively, we can take advantage of Eqs. (36) and (18) (with $K_1 = K_2 = 0$) to let Eq. (41) become,

$$[A_1A_2(x^2y^2 + \gamma_2x^2y + \gamma_1xy^2 + \gamma_1\gamma_2xy) - A_2\gamma_1^2(y + \gamma_2)\lambda y] D + A_1\gamma_2^2x^2 + A_2\gamma_1^2y^2 + \gamma_1^2\gamma_2^2z = 0. \quad (43)$$

Set $\gamma_1 = \gamma_2 = 1$. The elimination of x and y between Eqs. (42-43) yields a degree 7 polynomial condition for D ,

$$\begin{aligned} \mathcal{P}(D, z, A_1, A_2, \lambda) \equiv & A_2^2(A_1 + 4\lambda)^2 [(z + \lambda)^2 + A_1z] [(z + \lambda + A_2)^2 + A_1(z + A_2)] D^7 - \\ & 4A_2(A_1 + 4\lambda) [(z + \lambda)^2 + A_1z] [A_1A_2^2 + 5A_1A_2\lambda + 8A_2^2\lambda + 12A_2\lambda^2 + 4\lambda^3 + (-3A_1A_2 - 4A_2^2 + \\ & 4A_1\lambda + 4A_2\lambda + 4\lambda^2)z - 4(A_1 + 2A_2 + \lambda)z^2 - 4z^3] D^6 + \dots - 64z(A_1 + A_2 + 20\lambda + 16z) D + 256z = 0, \end{aligned} \quad (44)$$

which is too cumbersome to be listed here entirely. A factor $[(z + \lambda)^2 + A_1z]$ forces its coefficients for both D^7 and D^6 to vanish when $z = \eta_0$, see Eq. (40). Hence two roots D diverge at the expected one-body threshold. We also notice that for $z = 0$ the two lowest degree coefficients of \mathcal{P} vanish, hence a double root $D = 0$ occurs. But, for the sake of simplicity in this Section, we shall not elaborate much on the exact nature of this two-body threshold singularity for this second model. Similarities with the behavior of the first model around $z = 0$ are likely. In the following we rather study in some detail the singularity at $z = \eta_0$.

The degree 7 for D is familiar from the model of the previous Section. But the degree for z is now 5 rather than 4. We verified that the limit $\lambda \rightarrow 0$ factorizes $\mathcal{P}(D, z, A_1, A_2, \lambda)$ into a factor z and a polynomial with degree 4 for z .

It is convenient to set special values for a numerical investigation, for instance $a_1 = \gamma_1 = A_1 = \gamma_2 = 1$ and $a_2 = A_2 = \lambda = 2$. The full polynomial then reads,

$$\begin{aligned} \mathcal{P} = & 3(1+z)(4+z) [27(3+z)(6+z)D + 12(-108 - 9z + 14z^2 + 2z^3)] D^6 - \\ & 4(-2808 + 477z + 5984z^2 + 3480z^3 + 690z^4 + 44z^5) D^5 + 8(-584 + 1760z + 3323z^2 + 1387z^3 + 200z^4 + 8z^5) D^4 - \\ & 8(-140 + 1195z + 1471z^2 + 420z^3 + 32z^4) D^3 + 32(-4 + 107z + 82z^2 + 12z^3) D^2 - 16z(43 + 16z) D + 64z. \end{aligned} \quad (45)$$

Here, the bound state lies at $\eta_0 = -1$ with $\omega_0 = i$. The second solution, $\omega_0 = -2i, \eta_0 = -4$, of Eqs. (39-40) violates the condition $\Re x > 0$, hence pertains to an unphysical sheet.

The 7 trajectories shown in Fig. 6 are those of the roots of \mathcal{P} , Eq. (45), when $\Re z$ runs from -7.5 to $+4$. This range suffices here to obtain a reasonable estimate of the root behavior when the energy runs from $-\infty$ to $+\infty$. For the sake of graphical convenience, a renormalization $D/(1+|D|)$ forces large D 's back to the trigonometric circle. Also a small imaginary part $\Im z = .2$ is set to enforce the rule $\Im D < 0$. Black dots (or lines when nearing dots fuse) correspond to $\Re z < -4.1$. Green and red ones correspond to $-3.9 < \Re z < -1.1$ and $-0.9 < \Re z$, respectively. Finally, blue and yellow ones investigate neighborhoods, $-4.1 < \Re z < -3.9$ and $-1.1 < \Re z < -0.9$, of expected singularities at $z = -4$ and $z = -1$, respectively. It turns out that Fig. 6 does not yield much information out of such "blue" and "yellow" segments, although it is clear that only two "loops" satisfy both rules $\Im D < 0, \forall \Re z$ and $\lim_{|z| \rightarrow \infty} D = 0$. Clearly, for a thorough investigation of all branchings and divergences, we should eliminate D between \mathcal{P} and its derivative $\partial\mathcal{P}/\partial D$, then study the neighborhoods of all the roots of the obtained resultant,

$$\begin{aligned} \mathcal{R} = & z(1+z)^2(2+z)(3+z)(4+z)^2(6+z)(32+7z)^2 \times \\ & (2426112 + 17293824z + 54026784z^2 + 121209152z^3 + 233641545z^4 + 328920768z^5 + \\ & 307812074z^6 + 191171112z^7 + 79534245z^8 + 21923392z^9 + 3826944z^{10} + 380928z^{11} + 16384z^{12})^3. \end{aligned} \quad (46)$$

This straightforward but lengthy task gives too cumbersome results to be published here, naturally. Still, it might be useful to compare Fig. 6 with a superposition of Figs. 2 and 11, keeping in mind that symmetry breaking double roots of the previous model will now be disentangled. Indeed, under the already mentioned two criteria, namely i) $D \rightarrow 0$ if $|z| \rightarrow \infty$, and ii) $\Im D < 0$, only the “tiny” loops selected from Figs. 2 and 11 survive. Letting $\Im z \rightarrow 0$, we obtained graphical evidence that such two loops grow in such a way that their “blue” and “yellow” segments show the diverging roots predicted from the factor $(1+z)(4+z)$ in front of D^7 and D^6 . With the same renormalization $D/(1+|D|)$, Fig. 7 confirms that two branches only are compatible with rules i) and ii), when we freeze $\Re z = -1$ and let $\Im z > 0$ run. One of the “good” candidate roots diverges for $z = -1$, see the green segment in the lower left part of Fig. 7. The other “good” candidate, $D_1 \simeq .31 - .21i$, see the small green segment at the beginning of the smallest trajectory in the lower right angle of Fig. 7, is a simple root as a function of z in this area, and deserves little comment. The diverging root, however, because of its quadratic branching, deserves a study of its reciprocal, $d \equiv D^{-1}$. We set $z = -1 + Z$ and expand \mathcal{P} , Eq. (45), at lowest orders with respect to d and Z ,

$$d^7 \mathcal{P}(d^{-1}, Z - 1, A_1 = 1, A_2 = 2, \lambda = 2) = 270(2d^2 + 9Z) + \mathcal{O}(Zd). \quad (47)$$

The neglected term is of order $Z^{3/2}$, because, obviously, the leading order of the double root is $d = \pm 3(-Z)^{1/2}/\sqrt{2}$, real below and imaginary above threshold, respectively. A similar, straightforward argument for the vicinity of the additional, but unphysical threshold at $z = -4$ yields the leading order $d = \pm 3(-4-z)^{1/2}/(2\sqrt{2})$.

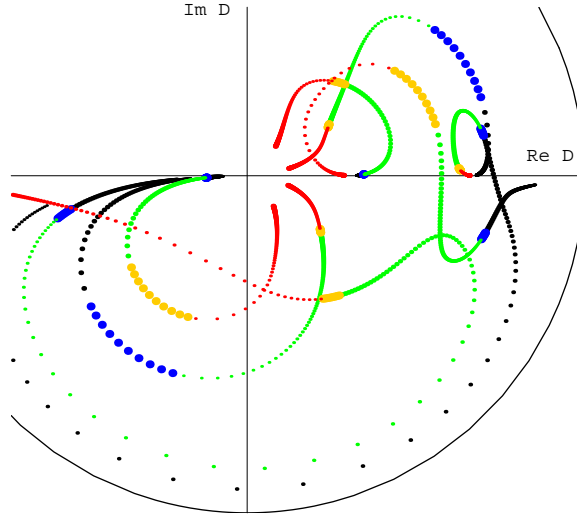


FIG. 6. Complex D -plane. Trajectories of the 7 roots of Eq. (45) when $-7.5 \leq \Re z \leq 4$ and $\Im z = .2$. Black dots or lines correspond to $\Re z < -4.1$. Blue, green, yellow and red ones correspond to $-4.1 < \Re z < -3.9$, $-3.9 < \Re z < -1.1$, $-1.1 < \Re z < -0.9$, and $-0.9 < \Re z$, respectively. Only two trajectories always keep $\Im D < 0$ and cancel D when $|z| \rightarrow \infty$.

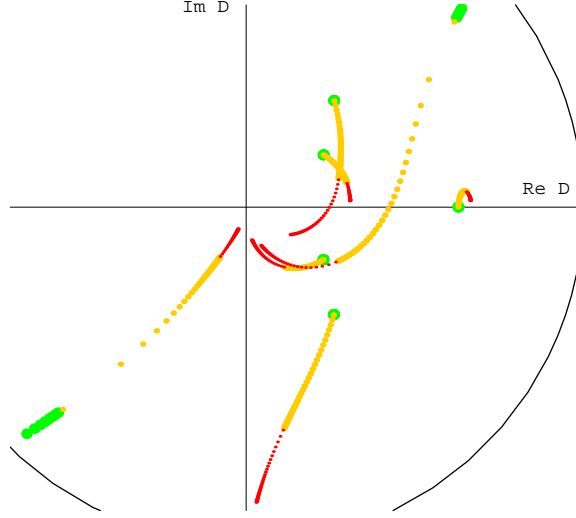


FIG. 7. Complex D -plane. Trajectories of the 7 roots of Eq. (45) if $\Re z = -1$. Green, yellow and red mean $0 < \Im z < .01$, $.01 < \Im z < 2$ and $2 < \Im z < 8$, respectively. Again, only two trajectories maintain $\Im D < 0$ and cancel D when $|z| \rightarrow \infty$.

Among all the singularities of this second model, we shall mainly discuss the physical threshold $z = -1$. Eliminate z between Eq. (42a) and Eq. (42b), or, equivalently, subtract the equations, Eqs. (37), from each other, hence

$$a_2 \omega_2 J_2 \frac{d\omega_2}{dJ_2} = a_1 \omega_1 \mathcal{I}_1 \frac{d\omega_1}{d\mathcal{I}_1}, \quad (48)$$

a relation similar to Eq. (16). To prove the statement that the static HF energy η_0 indeed defines a threshold solution of the TIMF equations, Eqs. (37), it is enough to set $\eta_1 \rightarrow \eta_0$, $\eta_2 \rightarrow 0$ and $z \rightarrow \eta_0$. This automatically induces $z - a_1 \omega_1^2 - a_2 \omega_2^2 \rightarrow 0$, naturally. Set $\gamma_1 = \gamma_2 = 1$, for a trivial scaling. Then Eq. (48) reads,

$$\frac{A_2 y^2 (1 + y)}{1 + 2y} = \frac{x [A_1 x (1 + x) - \lambda]}{1 + 2x}. \quad (49)$$

When $A_1 = 1$ and $A_2 = \lambda = 2$, we know that the limits of interest are $x \rightarrow 1$, $y \rightarrow 0$ and $z \rightarrow -1$. These satisfy the condition, $\Re x > 0$, hence only $\Re y$ must be investigated. Define $X = x - 1$ and $Z = z + 1$. Then Eq. (49) boils down to $2y^2 = X$, at leading orders in y and X . Accordingly, Eq. (42b), for instance, boils down to, $2y^2 + Z = 0$. For $z < -1$ (below threshold) the solution, $y \rightarrow \sqrt{(-z - 1)/2}$, is acceptable, with, simultaneously, $x \rightarrow -z$. For $z > -1$ (above threshold), however, we find that a small, but positive $\Im z$ is necessary to allow the condition $\Re y > 0$. This occurs because for $Z > 0$ the leading order, $y^2 \rightarrow -Z/2$, actually generates $\Im y$ only. An expansion up to higher orders, is thus necessary for the knowledge of $\Re y$. A straightforward, but slightly lengthy calculation yields,

$$y = iZ' - \frac{i}{3}Z'^3 - \frac{2}{3}Z'^4 + \frac{13i}{18}Z'^5 + \mathcal{O}(Z'^6), \quad (50)$$

where Z' , a positive number, is defined as $Z' = \sqrt{Z/2} = \sqrt{(z + 1)/2}$. The “formal conjugate” of this expansion,

$$y = -iZ' + \frac{i}{3}Z'^3 - \frac{2}{3}Z'^4 - \frac{13i}{18}Z'^5 + \mathcal{O}(Z'^6), \quad (51)$$

also holds, naturally. (Equivalently, it means the opposite choice of Z' , namely $Z' = -\sqrt{Z/2}$.) Both expansions induce a negative $\Re y$ as long as Z is real and positive. The sign of this $\Re y$ can be easily reversed, however, as soon

as, above that threshold $z = -1$, an imaginary part $\Im z$ is implemented. Another slightly cumbersome calculation defines, upon taking advantage of either Eq. (50) or Eq. (51), the condition for the border at which one of such roots acquires a positive real part. This is illustrated by Fig. 8. Near to that threshold $z = -1$, the leading orders of the border condition give, $(\Im z)^2 = \frac{2}{9}(\Re z + 1)^5$. Other numerical values for the parameters γ_i, A_i etc. modify the numerical analysis, naturally, but leave intact the conclusion, namely that $|\Im z|$ must have at least a non vanishing value above the threshold if one needs one of these two roots to be compatible with the condition, $\Re y > 0$.

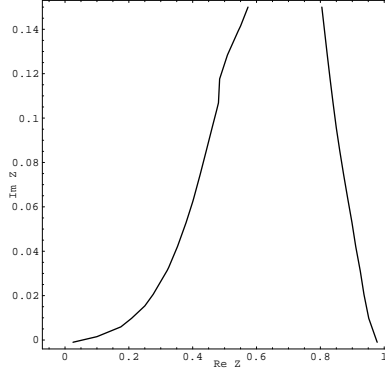


FIG. 8. Complex $Z \equiv z + 1$ -plane. Below the plotted line, both roots described by Eqs. (50-51) show $\Re y < 0$. Above that line, one of them shows $\Re y > 0$. The line contains both thresholds $Z = 0$ and $Z = 1$.

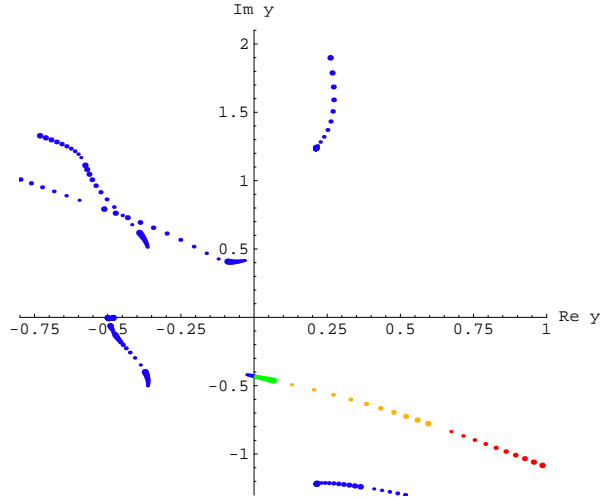


FIG. 9. Complex y -plane. Trajectories of y when $\Re z = -.6$ and $\Im z$ increases from 0. Blue lines are trajectories for which either $\Re x$ or $\Re y$ or both are negative. Only one branch, that long one in the lower right quadrant, survives the double condition, $\Re x > 0, \Re y > 0$. Tiny blue segment, $0 < \Im z < .03$. Green segment, $.04 < \Im z < .2$. Orange one, $.3 < \Im z < 1.8$. Red one, $2 < \Im z < 4$.

We show on Figure 9 the trajectories of y for $0 < \Im z < \infty$ when $\Re z = -.6$ is frozen at an intermediate value between the thresholds $z = -1$ and $z = 0$. Only one branch is of interest, because all the other branches either stay in the $\Re y < 0$ sector or the x partner root shows $\Re x < 0$. The tiny blue segment at the beginning of this branch corresponds to $\Im z < .03$, imaginary parts too small for letting y acquire a positive real part, see Figure 8.

IV. A THEOREM

We return to the case where N is any finite particle number. The two-body interaction $V = \sum_{i>j} v_{ij}$ contained in the physical Hamiltonian H is assumed to be made of short ranged potentials v_{ij} . Then the TIMF mean fields U_i are also short ranged. For details of a further antisymmetrization with identical fermions, where the mean potential will be the same U for all particles, we refer to [8]; the short range of U remains, whether one considers its direct or exchange part. At present we still retain the case of distinct particles. Eqs. (3) read again,

$$(\eta_i - t_i - U_i)|\varphi_i\rangle = |\chi_i\rangle, \quad \langle\varphi'_i|(t_i - U_i) = \langle\chi'_i|, \quad (52)$$

with

$$\eta_i = z - \frac{\langle\phi'|H|\phi\rangle}{\langle\phi'|\phi\rangle} + \frac{\langle\varphi'_i|(t_i + U_i)|\varphi_i\rangle}{\langle\varphi'_i|\varphi_i\rangle}. \quad (53)$$

Notice that we now process a generalized argument, since we can also study non diagonal elements $\langle\chi'|(z - H)^{-1}|\chi\rangle$ where χ and χ' are products made of orbitals χ_i and χ'_i , respectively. The Euclidian restriction is not implemented any more. The trial functions ϕ and ϕ' are the products made of orbitals φ_i and φ'_i , respectively. All such quantities and wave functions depend on z , but we stress here that, because of the short range of U_i , the spectrum of $h_i = t_i + U_i$ has a fixed continuum, extending from 0 to $+\infty$ on the real axis of the η_i complex plane. In general U_i is complex and the poles of $(\eta_i - h_i)^{-1}$ need not be real; as a matter of fact they move as functions of z (and of the choices of χ and χ'). But the continuum cut for the spectrum of h_i remains always the same. It is therefore legitimate to ask the question “what happens if one of the η_i ’s vanishes, hitting the threshold of the continuum of h_i ?”. Incidentally, it will be noticed that there are many trajectories (sheets) of such η_i ’s as functions of z . The multiplicity comes not only from the existence of N “momenta”, $\omega_i \propto \pm\sqrt{\eta_i}$, with their \pm ambiguity [12], but it is also due to the nonlinearity of the mean field theory. For instance, in our second model, we found seven sheets, see the seven roots for each quantity $D(z)$, $x(z)$, $y(z)$ driven by z .

As a preliminary remark, we use Eqs. (53) to notice that the mismatch between any propagation energy η_i and the corresponding self energy $\langle\varphi'_i|(t_i + U_i)|\varphi_i\rangle/\langle\varphi'_i|\varphi_i\rangle$ does not depend on i . Furthermore we can take advantage of Eqs. (52) to relate the self and propagation energies as,

$$\frac{\langle\varphi'_i|(t_i + U_i)|\varphi_i\rangle}{\langle\varphi'_i|\varphi_i\rangle} = \eta_i + \frac{\mathcal{K}_i d\eta_i}{d\mathcal{K}_i}, \quad \mathcal{K}_i = \langle\chi'_i|(h_i - \eta_i)^{-1}|\chi_i\rangle = -\langle\varphi'_i|\chi_i\rangle = -\langle\chi'_i|\varphi_i\rangle. \quad (54)$$

In other terms, the mismatch is measured by the ratio $\langle\chi'_i|\varphi_i\rangle/\langle\varphi'_i|\varphi_i\rangle = \langle\varphi'_i|\chi_i\rangle/\langle\varphi'_i|\varphi_i\rangle$ as a function of η_i . When calculated at self consistent $\eta_i(z)$ ’s, such ratios do not depend on i any more.

Assume that the special vanishing η_s reads $\eta_s = i\varepsilon^2$, where ε is a real, positive infinitesimal. This means that we select in the z complex plane a trajectory which in turn induces an η_s trajectory leading to retarded, outgoing boundary conditions for that special φ_s and its partner φ'_s . For the sake of simplicity, set the inverse mass coefficient a_s to unity, or, equivalently, renormalize η_s and U_s accordingly. In physical three dimensions, the partial wave components $\varphi_{s\ell}$ are described by differential equations of the form,

$$-\frac{d^2\varphi_{s\ell}}{dr^2} + \left[\frac{\ell(\ell+1)}{r^2} + U_{s\ell}(r) - i\varepsilon^2 \right] \varphi_{s\ell}(r) = \chi_{s\ell}(r) - \sum_{\ell'} \int_0^\infty dr' U_{s\ell\ell'}(r, r') \varphi_{s\ell'}(r'), \quad \forall \ell, \quad (55)$$

where $U_{s\ell\ell'}$ is a short notation accounting for, if necessary, partial wave coupling and/or non local parts of U_s . The source term χ_s is expanded in partial waves as well, naturally. It is then convenient to denote the right hand sides of Eqs. (55) as source terms $\xi_{s\ell}(r)$. These are short ranged, obviously again. Similar equations hold for φ'_s .

For each ℓ let $\sigma_{s\ell}(r)$ be the regular solution, usually normalized as $\sigma'_{s\ell}(0) = 1$, of the homogeneous, left hand side of Eqs. (55). The short range of U_s , and similar short ranges assumed for χ and χ' , make it that, when $r \rightarrow \infty$, then $\varphi_{s\ell}(r)$ becomes $\simeq \exp[(i-1)\varepsilon r/\sqrt{2}] \int_0^\infty dr' \sigma_{s\ell}(r') \xi_{s\ell}(r')$, with a similar asymptotic formula for $\varphi'_{s\ell}$. Let C , a real

and strictly positive number, be any convenient lower bound for the absolute values of these integrals $\int \sigma \xi$ and $\int \sigma \xi'$ in a neighborhood of $\varepsilon \rightarrow 0$. This C exists, since such integrals are usually finite and non vanishing when $\varepsilon = 0$. It is clear that, as $\varepsilon \rightarrow 0$, there are no more any exponential decays or any asymptotic oscillations in the product $\varphi_s \varphi'_s$. Then, at this limit for ε , the integral $\langle \varphi'_s | \varphi_s \rangle$ diverges, while obviously an integral such as $\langle \chi'_s | \varphi_s \rangle$ remains finite. The “mismatch” cancels out.

This indicates that, for any $i \neq s$, the ratios $\mathcal{K}_i d\eta_i/d\mathcal{K}_i$ vanish simultaneously at their respective energies η_i . Besides threshold limits for each η_i , there is an easy interpretation for such a situation, namely, each among such $N - 1$ propagation energies converges towards a bound state energy of its h_i . Indeed, let de_i be an infinitesimal difference between η_i and an isolated eigenvalue of h_i . Then it is trivial, in an energy representation with biorthogonal eigenstates of h_i , to see that \mathcal{K}_i diverges at order $(de_i)^{-1}$, while $d\mathcal{K}_i/d\eta_i$ diverges at order $(de_i)^{-2}$.

The situation is thus representative of a Hartree(-Fock) solution for the $N - 1$ particle system. This is confirmed by the observation that, since $\langle \varphi'_s | \varphi_s \rangle$ diverges, the potential $U_{i/s}$ induced by particle s upon any particle $i \neq s$ vanishes. Indeed, the short range of v in the formula,

$$U_{i/s}(r_i) = \frac{\int dr' v_{is}(r_i - r') \varphi'_s(r') \varphi_s(r')}{\langle \varphi'_s | \varphi_s \rangle}, \quad (56)$$

makes the numerator converge $\forall r_i$, while the denominator diverges. Any matrix element $\langle \varphi'_i \varphi'_s | v | \varphi_i \varphi_s \rangle$ will vanish too, for the same reason. Furthermore, the full matrix element $\langle \phi' | H | \phi \rangle / \langle \phi' | \phi \rangle$ can always be split as,

$$\frac{\langle \phi' | H | \phi \rangle}{\langle \phi' | \phi \rangle} = \frac{\langle \phi'_{-s} | H_{-s} | \phi_{-s} \rangle}{\langle \phi'_{-s} | \phi_{-s} \rangle} + \frac{\langle \varphi'_s | (t_s + U_s) | \varphi_s \rangle}{\langle \varphi'_s | \varphi_s \rangle}, \quad (57)$$

where the subscript $-s$ refers to the subsystem where particle s is removed. At the limit under study, both η_s and $\mathcal{K}_s d\eta_s/d\mathcal{K}_s$ vanish. Hence, according to Eq.(54), the self energy for particle s vanishes and the full matrix element $\langle \phi' | H | \phi \rangle / \langle \phi' | \phi \rangle$ reduces to the subsystem value, $\langle \phi'_{-s} | H_{-s} | \phi_{-s} \rangle / \langle \phi'_{-s} | \phi_{-s} \rangle$. Furthermore, setting $i = s$ in Eq.(53), we find that $z \rightarrow \langle \phi'_{-s} | H_{-s} | \phi_{-s} \rangle / \langle \phi'_{-s} | \phi_{-s} \rangle$. The threshold for the continuum of particle s in the z -plane corresponds to the Hartree(-Fock) binding energy of the subsystem.

Conversely, if z converges towards a Hartree(-Fock) bound state energy of an $N - 1$ particle system, it is easy to verify that at least one solution of the TIMF equations for the N particle system consists in a threshold wave for the additional particle, as a spectator of the static solution for the subsystem.

Notice that several special particles, not just one, can be forced into their continuum thresholds simultaneously. For instance, if particle s and s' are such that $\eta_s = \eta_{s'} = 0$, then all potentials $U_{i/s}$ and $U_{i/s'}$, including $U_{s/s'}$ and $U_{s'/s}$, vanish, and $z = \langle \phi'_{-s-s'} | H_{-s-s'} | \phi_{-s-s'} \rangle / \langle \phi'_{-s-s'} | \phi_{-s-s'} \rangle$, a subsystem energy for $N - 2$ particles.

It can be also noticed that such singularities do not depend upon the source terms χ and χ' . Indeed, the locations of such thresholds derive from homogeneous equations, where only H appears.

The present theorem can be phrased in a way which generalizes the theorem of [10]: not only the mean field binding energies of a system of N particles define singularities of the TIMF propagator, but the mean field binding energies of its subsystems define thresholds of cuts where the additional particles become unbound.

V. DISCUSSION AND CONCLUSION

There are two parts in this work, namely on the one hand a couple of very special, analytical models, see Sections II and III, and on the other hand a theorem of a more general validity.

The systems described by our models are physically trivial, since they make non interacting particles. But their mathematical interest is different. As stated at the beginning of this work, it is important, for large particle numbers, to validate the replacement of convolutions by straight products, and our models allow a detail study of all singularities and nonlinearities introduced by the mean field approximation. We investigated three representations, namely what happens in, i) the z -plane (propagation energy), see for instance Figure 4, ii) the D -plane (TIMF amplitude), see for instance Figure 1, iii) pseudo momentum planes, such as, for instance the case of $x = -i\sqrt{\eta_1/a_1}$, see Figure 5. Since our models automatically implement an analytic continuation from physical to unphysical sheets, there is no cut to consider in the pseudo momentum complex planes. It is obvious, however, that for both pseudo momenta x and y the imaginary axis represents both rims of the cut which would be necessary in their respective η -plane. Accordingly, see for instance Figure 8, values of z for which the real part of a pseudo momentum vanishes, or identically for which a propagation energy $\eta(z)$ becomes real and positive, make cuts in the z representation. The zoology of the TIMF solutions turns out to be surprisingly rich. The main two conclusions provided by the models can be listed as follows,

i) except when the many-body propagation energy z has too small an imaginary part, the TIMF equations always generate at least one branch of solutions where each single particle undergoes a retarded propagation and the TIMF amplitude D shows all suitable properties needed for a reasonable approximation of a Green's function matrix element, ii) the threshold of a single particle continuum induces the threshold of a cut singularity in the z representation; if one calls “projectile” that special particle becoming unbound, and “target” the system made by the other particle, the corresponding threshold value for the full propagation energy z is the binding energy of the “target”.

The theorem derived in Section IV, valid for any particle number $N \geq 2$, extends this numerical and analytical evidence. Hence the mean field theory of collisions mimicks the connection between singularities of the inhomogeneous problem $(z - H)|\Psi\rangle = |\chi\rangle$ and the solutions of the homogeneous Schrödinger equation $(E - H)|\Psi\rangle = 0$. At this stage of our work, the similarity is restricted, however: we considered only partitions where a “target” is surrounded by one or several unbound particles, and we have not proven thresholds defined by mean field energies of partitions $N_1 + N_2 = N$, $N_1 \geq 2$, $N_2 \geq 2$, into two clusters, each of them carrying its full internal energy. Nor have we considered even finer partitions $N_1 + N_2 + N_3 = N$, with $N_1 \geq 2$, $N_2 \geq 2$, $N_3 \geq 2$, and so on. Last but not least, the present work lacks a clear description of the shapes of the cuts beyond their thresholds. The preliminary result obtained at the stage of Figure 8, with a “border equation” like $(\Im z)^2 = \frac{2}{9}(\Re z + 1)^5$, is an omen of subtle arguments yet to be phrased.

Despite such questions still open, the TIMF approximation now appears like a theory of collisions endowed with properties, such as poles and thresholds, with sound interpretations in terms of Hartree-(Fock) energies of subsystems. The special role played by single particle energy propagators $(\eta - h)^{-1}$ in the definition of such properties is a logical consequence of the factorization of trial wave functions, an essential ingredient of practical approximations. With the present and foregoing studies, TIMF appears as a reliable and practicable alternative to resonating group (RGM) or generator coordinate (GCM) studies for application in nuclear astrophysics where there is still a demand for microscopic rather than phenomenological calculations of processes relevant to element synthesis.

Acknowledgement A.W. thanks Service de Physique Théorique, Saclay, for its hospitality during part of this work.

-
1. P.A.M. Dirac, Proc. Cambridge Phil. Soc. **26** (1930) 376; P. Bonche, S. Koonin and J.W. Negele, Phys.Rev. **C 13** (1976) 1226; K. Goeke, R.Y. Cusson, F. Grümmer, P.-G. Reinhard and H. Reinhardt, Prog. Theor. Phys. [Suppl.] **74, 75** (1983) 33
 2. H. Reinhardt, Nuclear Physics A **390** (1982) 70
 3. J. W. Negele and H. Orland, *Quantum Many-Particle Systems* (Addison-Wesley, 1988)
 4. H. Reinhardt, Fortschr. d. Physik **30** (1982) 127
 5. J. P. Blaizot and G. Ripka, *Quantum Theory of Finite Systems* (MIT Press, 1986)
 6. B. Giraud, M. A. Nagarajan and I. J. Thompson, Ann. Phys. (N.Y.) **152** (1984) 475; B. Giraud and M. A. Nagarajan, Ann. Phys. (N. Y.) **212** (1991) 260
 7. J. Schwinger, Phys. Rev. **72** (1947) 742; Ch.J. Joachain, *Quantum Collision Theory* (North Holland, Amsterdam, 1975); T. Wu and T. Ohmura, *Quantum Theory of Scattering* (Prentice Hall, 1962)
 8. J. C. Lemm, Ann. Phys. (N.Y.) **244** (1995) 136
 9. J. Uhlig, J.C. Lemm and A. Weiguny, Eur. Phys. J. **A2** (1998) 343
 10. B.G. Giraud, Prog. Theor. Phys. **88** (1992) 1147
 11. B.G. Giraud, Physica **19 D** (1986) 112
 12. R.G. Newton, *Scattering Theory of Waves and Particles*, (MacGraw-Hill, New York, 1966)
 13. B.G. Giraud, M.A. Nagarajan and A. Weiguny, Phys. Rev. **C 35** (1987) 55

VI. APPENDIX: THE SYMMETRY BREAKING BRANCH OF THE FIRST MODEL

For the symmetry breaking sector of the first model, we again set $a_i = \gamma_i = 1$, scaling x, y, z and ensuring the factorization of the resultant, Eq. (22a). It is easy to analyze the singularities of the direct solution of Eq. (26a),

$$D_{bk} = 2 \pm 2 \left(\frac{z_{bk}}{1 + z_{bk}} \right)^{1/2}, \quad (58)$$

in terms of one cut from -1 to 0 in the complex z -plane, or, alternately, two cuts from $-\infty$ to -1 and from 0 to $+\infty$, and observe that the square root singularity at $z = 0$ seems to represent a very traditional threshold singularity. Less physical, the rôle of $z = -1$ is to reflect the discriminant $\Delta_2 = 4z/(1+z)$ of Eq. (26a).

In the forthcoming Figures, we keep $\theta = 1$, as a natural scale for energies and inverse amplitudes. Fig. 10 shows the graph of z_{bk} when D_{bk} is real and takes on all values from $-\infty$ to $+\infty$. The symmetry axis at $D = 2$ is obvious from Eq. (27). Since the physical amplitude is negative when z is negative, the right lower branch of the graph is clearly unphysical, while the left lower branch is a reasonable candidate for approximations. (Notice, however, that no real estimate of the amplitude is offered for $-1 \leq z \leq 0$.) In turn, the right upper branch is also ruled out, as \mathcal{D} must vanish when $z \rightarrow +\infty$. This leaves the left upper branch as a tolerable candidate for physical approximates of the real (principal) part of \mathcal{D} when z is positive.

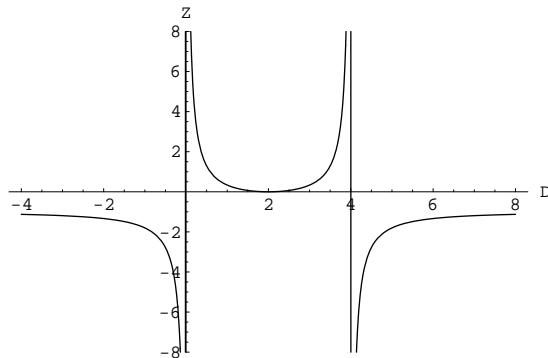


FIG. 10. Scaled energy z (unit θ) as a function of the “symmetry breaking” amplitude D (unit $1/\theta$).

Rather than considering inverse functions $z(D)$, we then show in Figs. 11-12 the trajectories, in a complex plane “ D ”, of the solutions of Eq. (26a) when $\Re z$ takes on all values from $-\infty$ to $+\infty$ and $\Im z$ is frozen at some fixed value Γ . The physical situation corresponds to $\Gamma = 0^+$, naturally, but Figs. 11-12 use larger values of Γ for graphical convenience. For Fig. 11, we use $\Gamma = .075$ and $\Gamma = .4$, which generate for D_{bk} two “outer loops” and two “inner loops”, respectively. The rôle of $D = 2$ as a symmetry center is obvious. The shrinking of the loops when Γ increases comes from the fact that, as $|z| \rightarrow \infty$, the dominant part of the symmetry breaking equation is $D(D - 4) = 0$. Conversely, the evolution of such loops into “angles” when $\Gamma \rightarrow 0$ is transparent on Fig. 12, obtained with $\Gamma = .02$. Only those solutions which lie in the lower half plane can be retained as physical candidates, according to the condition “if $\Im z > 0$, then $\Im D < 0$.” Hence the general physical behavior of D_{bk} is as follows:

- when z is real and increases from $-\infty$ to -1 , then D decreases from 0^- to $-\infty$,
- when z is real and increases from -1 to 0 , then D varies from $2 - i\infty$ to 2 ,
- when $\Im z = 0^+$ and $\Re z$ increases from 0 to $+\infty$, then D decreases from $2 + i0^-$ to $i0^-$. This infinitesimal imaginary part hints that D_{bk} can at best approximate the principal part of \mathcal{D} . This was already deduced from Fig. 10.

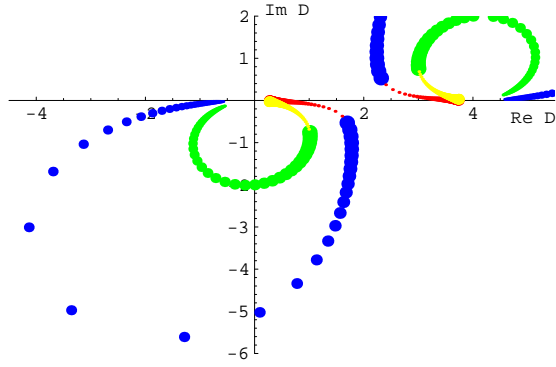


FIG. 11. Complex D -plane. Trajectories of symmetry breaking D when $\Im z = .075$ (outer loops) and $\Im z = .4$ (inner ones). For $\Im z = .075$, blue dots growing for $\Re z$ growing between $-\infty$ and 0^- and red ones growing for $\Re z$ growing from 0^+ to $+\infty$. For $\Im z = .4$, blue and red replaced by green and yellow, respectively.

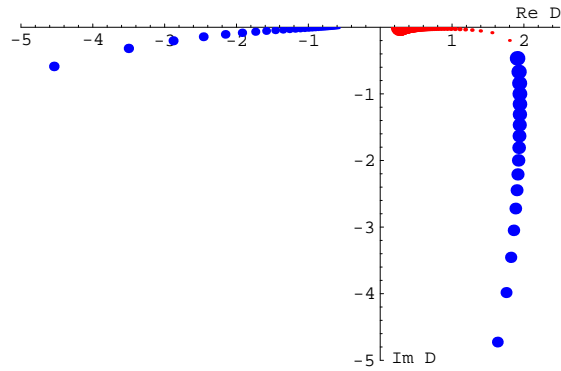


FIG. 12. Complex D -plane. Lower loop trajectory of D_{bk} when $\Im z = .02$ Blue dots growing for $\Re z$ growing between $-\infty$ and 0^- . Red ones growing for $\Re z$ growing from 0^+ to $+\infty$.

The “breaking” factor of the factorizing resultant between Eqs. (20) reads,

$$x^4 - 2x^3z - x^2z - 2xz(1+z) - z(1+z) = 0, \quad (59)$$

keeping in mind that its roots must be paired as (x, y) . Fig. 13 displays a contour plot of the product of the corresponding 4 real parts of the roots as functions of z . The corresponding cut in the z -plane is the border between the light grey and the darker grey areas. It is now made of two branches. The right hand branch, while not located on the real axis of the z -plane, again contains the two-body threshold $z = 0$.

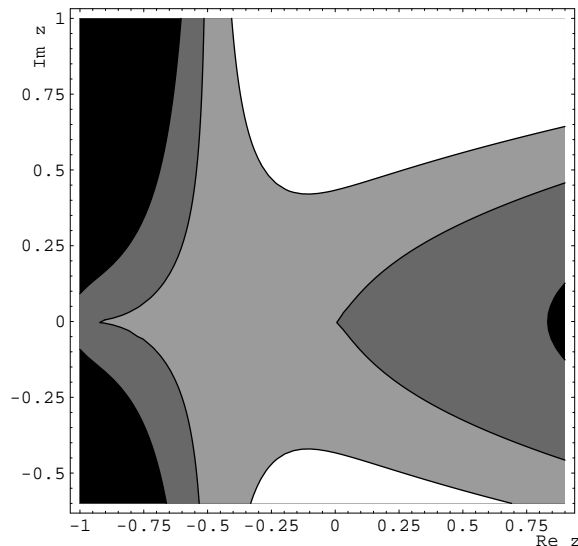


FIG. 13. Complex z -plane. Cuts caused by the condition $\Re x = 0$ for symmetry breaking roots. The cuts are the borders between light grey and darker grey areas.

Then Fig. 14 shows the trajectories of the 4 roots when we freeze $\Re z = 0.1$ and let $\Im z$ run from -1 to $+1$, allowing z to cross twice the right hand side cut shown by Fig. 13. The sizes of the dots are coded like those of Fig. 5: minimal for $\Im z = -1$, growing until $\Im z = 0$, minimal again for small positive values of $\Im z$, growing again until $\Im z = 1$. The “vertical” branch on the right hand side of Fig. 14 has the unsatisfactory property, that its “ y -partner” according to Eq. (22b), is the loop like, tiny branch on the left hand side of Fig. 14. Hence $\Re x \Re y < 0$. In turn, the two “horizontal” branches on Fig. 14 are “ x - y ” partners and are partly located inside the right hand side of the complex x, y -plane. But actually the double condition, $\Re x > 0$, $\Re y > 0$, is never satisfied. It must be concluded that the symmetry breaking sector is unphysical.

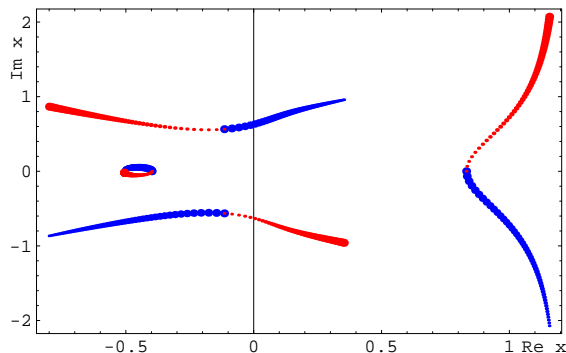


FIG. 14. Complex x -plane. Trajectories of the symmetry breaking x 's when $\Re z = 0.1$, while $\Im z$ runs through one of the cuts shown by Fig. 13. Blue dots growing when $\Im z$ grows from -1 to 0 . Red dots growing when $\Im z$ grows from 0 to 1 .

A trivial manipulation of Eqs. (20) shows that the pairing of roots, for this sector and such special parameters, follows the rule,

$$xy = z - x - y, \quad \text{hence} \quad y = \frac{z - x}{x + 1}, \quad (60)$$

which is its own inverse transform, naturally. The rule is equivalent to Eq. (22b), but simpler. Then if one defines $s \equiv x + y$, it is easy to reduce Eq. (59) into,

$$(z - s)^2 = z(z + 1), \quad \text{or} \quad z - s = \pm[z(z + 1)]^{1/2}, \quad (61)$$

while shortening Eq. (60) into,

$$xy = z - s = \pm[z(z + 1)]^{1/2}. \quad (62)$$

This means that Eq. (59) factorizes into two distinct equations,

$$x^2 - x \left[z - (z + z^2)^{1/2} \right] + (z + z^2)^{1/2} = 0, \quad (63a)$$

$$x^2 - x \left[z + (z + z^2)^{1/2} \right] - (z + z^2)^{1/2} = 0. \quad (63b)$$

It is easy to verify that each of these is invariant under the transform, Eq. (60), hence each yields a pair (x, y) . A detailed analysis of all cases for such equations is trivial, but too lengthy to be published. Rather, it is enough and easy, actually, to set $\Im z = 0$, and plot, for instance for Eq. (63a), its two numerical roots as functions of z . It turns out that at least one of the roots has always a negative real part. The same phenomenon occurs for Eq. (63b). All told, the symmetry breaking sector does not respect the constraints requested simultaneously for $\Re x$ and $\Re y$.